

The Self-Consistent Field Method Applied to Simulated Dark Matter Haloes

Ben Lowing^{1*}, Adrian Jenkins¹, Vincent Eke¹ and Carlos Frenk¹

¹*Institute for Computational Cosmology, Department of Physics, University of Durham, South Road, Durham, DH1 3LE, UK*

Accepted ... Received ... in original form ...

ABSTRACT

We apply the self-consistent field (SCF) method to create a time-evolving density/potential expansion approximation of the late growth of simulated N-body dark matter haloes. We demonstrate how the potential of a halo from the Aquarius Project can be accurately represented by a small number of basis functions. We explore the level of accuracy of the technique as well as some of its limitations. We find that the number of terms included in the expansion must be large enough to resolve the large-scale distribution and shape of the halo but, beyond this, additional terms result in little further improvement. Particle and subhalo orbits can be integrated in this realistic, time varying halo potential approximation, at much lower cost than the original simulation, with high fidelity for many individual orbits, and a good match to the distributions of orbital energy and angular momentum. Statistically, the evolution of structural subhalo properties, such as mass, half-mass radius and characteristic circular velocity, are very well reproduced in the SCF approximation over several gigayears. We demonstrate an application of the technique by following the evolution of an orbiting subhalo at much higher resolution than can be achieved in the original simulation. Our method represents a significant improvement over commonly used techniques based on static analytical descriptions of the halo potential.

Key words: dark matter: structure – galaxies: haloes – methods: numerical

1 INTRODUCTION

In the standard cosmological paradigm of structure formation (Λ CDM), dark matter haloes are built up through the repeated hierarchical merging of smaller haloes (White & Rees 1978; Frenk et al. 1985). These haloes provide the sites in which galaxies form. Any model of galaxy formation, be it an SPH simulation or a semi-analytical calculation, must include a description of the evolution of the halo in which the galaxy grows. These descriptions usually take the form of either N-body simulations, analytical potential profiles, or statistical merger trees. In this paper, we present a new way of characterising the evolution of dark matter haloes that can be employed in galaxy formation models, or to explore their small-scale structure.

Nearly all representations of haloes are motivated by cosmological N-body simulations. These are a powerful tool and have allowed us to gain insight into the non-linear stages of halo growth. The initial power spectrum of density fluctuations in the CDM cosmogony has power on all scales and this affects the internal evolution of haloes on a wide range of scales. However, investigating the structure and

substructure of halos requires simulations of ever increasing resolution and ever increasing computational expense. The state-of-the-art are the Aquarius simulations of galactic dark matter halos, the largest of which achieved a resolution of $\sim 10^3 M_\odot$ (Springel et al. 2008a). From these and other simulations (Stadel et al. 2009) we have learnt not only about the basic structure of haloes - that they have approximately universal density profiles well described by an NFW profile (Navarro et al. 1996, 1997) or that they are strongly triaxial in shape (Allgood et al. 2006; Bett et al. 2007; Hayashi et al. 2007) - but also about the properties of their small-scale structure (Springel et al. 2008a; Diemand et al. 2008; Vogelsberger & White 2010).

In spite of their impressive resolution, recent simulations have a number of limitations. Firstly, only a few examples have been calculated so far; secondly, their resolution is still below that required to follow the evolution of the smallest subhaloes, including those that host the ultrafaint dwarfs of the Milky Way; finally, they neglect the effects of baryons in the evolution of the main halo and its subhaloes.

The high cost of full simulations can be avoided by introducing approximations. A commonly used one is to assume a static analytical potential to represent the halo and then perform a live simulation of just the small-scale compo-

* E-mail: b.j.lowing@durham.ac.uk

nent of interest. Computational resources can then be targeted at that component and large numbers of resimulations performed. This method has been applied to a wide range of problems such as the orbits and evolution of subhaloes (Taylor & Babul 2001; Zentner & Bullock 2003; Peñarrubia & Benson 2005), the build-up of the galactic stellar halo (Bullock & Johnston 2005), the formation of streams (Peñarrubia et al. 2006), or the disruption and heating of disks (Benson et al. 2004).

Using an analytical potential allows the parameters of the dark matter halo to be varied in a way that cannot be done in full N-body simulations. The major shortcoming of this approach is that representing the halo with a simple analytical potential is unrealistic. Although recent studies have assumed slightly more complicated forms for the potential, such as axisymmetric NFW profiles (Peñarrubia et al. 2006) or triaxial NFW profiles (Law et al. 2009), they fail to include a realistic time evolution, as haloes grow in stages through mergers, or to account for changes in triaxiality with radius (Hayashi et al. 2007) and time.

In this paper, we present a more advanced approach for representing the potential of a halo, the self-consistent field (SCF) method (Clutton-Brock 1973; Hernquist & Ostriker 1992). The SCF method describes a potential and density field as a series expansion. It offers the means to create realistic approximations of a time varying halo potential, which can then be employed in resimulations. Previous work has used this method to perform N-body simulations (Weinberg 1996, 1999). SCF codes (also known as expansion codes) have the advantage of being efficient, of scaling linearly with the number of particles and of suppressing small-scale noise. Their main disadvantage is that the system of interest must closely match the basis functions; otherwise huge numbers of terms need to be included in the series. Originally used for modelling stellar systems (Earn & Sellwood 1995), the SCF method was recently applied by Choi et al. (2009) to simulate the potential of subhaloes, still assuming a static NFW potential for the host halo. Here, we propose the converse approach: we apply the SCF method to model the evolving host halo.

Our approach has the distinct advantage of providing a much more realistic description of a halo potential than a simple static analytical form, while still being inexpensive. The starting-point is a full N-body simulation. A set of coefficients is calculated that describes the halo with a chosen set of basis functions. Subsequently, an estimate of the halo density or potential at any point in space or time can be obtained by evaluating the appropriately weighted sum of the basis functions at that point.

There is a wide range of possible applications of this method. Problems to which it is ideally suited include: the orbits and stripping of subhaloes, the response of a light disk to the changing halo potential, the shape and precession of tidal streams, and the dynamics of satellite galaxies. In this paper, we focus on the first of these applications; we will explore the second in a later paper. Comparing orbits within a halo approximated by an SCF expansion to orbits calculated from the N-body halo serves as a demonstration of the method and provides a test of the accuracy of the approximation.

Limitations of the technique include the lack of back reaction of the halo potential when new components are

added. For example, if a model of a baryon disk is introduced, the associated reduction of the triaxiality at the centre of the dark halo (Debattista et al. 2008; Abadi et al. 2010; Bett et al. 2010) cannot be included in the SCF approximation. At present, the method does not treat the effect of dynamical friction on objects orbiting within the halo. Although this can, in principle, be implemented in the method, Boylan-Kolchin et al. (2008) find that, for subhalo-to-halo mass ratios less than 0.1 the decay of the subhalo orbit due to dynamical friction over a few Gyrs is small.

This paper is organised as follows. Section 2 describes the theory behind the SCF technique and how it has been applied to generate a representation of the density and potential of a simulated dark matter halo. Section 3 quantifies how well the SCF representation succeeds in recreating the orbits of both single particles and subhaloes. The latter part of the section carries out a comparison between the evolution of subhaloes in a full simulation and in the SCF potential. In Section 4, we use the SCF method to add a new subhalo into the halo and finally, in Section 5, we summarise our conclusions.

2 METHODOLOGY

We start by presenting a brief overview of the theory behind the SCF method and then describe the simulated haloes to which it has been applied and the considerations required in its application.

2.1 Self-Consistent Field Method

The self-consistent field (SCF) method was originally proposed by Clutton-Brock (1973) and has been typically used for studying stellar systems such as isolated galaxies. Hernquist & Ostriker (1992) (hereafter HO) further developed the technique and first applied it to galactic dynamics. The idea of the SCF technique is to expand the density and potential in a set of basis functions. The coefficients for the density can be found by summing over the particle distribution of a simulation. The corresponding coefficients for the potential are then obtained through solving Poisson's equation. Differentiation of the potential series gives the acceleration.

We perform our expansion in spherical polar coordinates with r the radial distance, θ the polar angle and ϕ the azimuthal angle. We start by considering the potential and density written as the biorthogonal series

$$\rho(r, \theta, \phi) = \sum_{nlm} A_{nlm} \rho_{nlm}(r, \theta, \phi), \quad (1)$$

$$\Phi(r, \theta, \phi) = \sum_{nlm} A_{nlm} \Phi_{nlm}(r, \theta, \phi), \quad (2)$$

where $\rho_{nlm}(r, \theta, \phi)$ and $\Phi_{nlm}(r, \theta, \phi)$ are the basis functions labelled by n, l, m . A pair of biorthogonal series are defined by the properties that

$$\int \rho(\mathbf{r})_{nlm} \rho(\mathbf{r})_{n'l'm'} d\mathbf{r} = \delta_{nn'} \delta_{ll'} \delta_{mm'}, \quad (3)$$

$$\int \Phi(\mathbf{r})_{nlm} \Phi(\mathbf{r})_{n'l'm'} d\mathbf{r} = \delta_{nn'} \delta_{ll'} \delta_{mm'}, \quad (4)$$

$$\int \rho(\mathbf{r})_{nlm} \Phi(\mathbf{r})_{n'l'm'} d\mathbf{r} = \delta_{nn'} \delta_{ll'} \delta_{mm'}. \quad (5)$$

Using a pair of biorthogonal series is not necessary, but it simplifies the calculation of the coefficients by allowing us to take the overlap of the density with the simpler potential basis functions. The biorthogonality property then ensures that each coefficient only depends on a single potential basis function and that there is no contribution to it from any of the other basis functions. The basis functions are chosen so that each pair of terms are a solution to Poisson's equation

$$\nabla^2 \Phi_{nlm}(r, \theta, \phi) = 4\pi G \rho_{nlm}(r, \theta, \phi), \quad (6)$$

with G the universal gravitational constant.

While we have a free choice of basis functions, it is desirable that lowest order terms be a good approximation to the system being modelled. This reduces the need to expand to high order to obtain a good fit. We have adopted basis functions from HO, where radial basis functions are based on the Hernquist profile (Hernquist 1990). A Hernquist profile is a reasonable fit to a dark matter halo, having an appropriate slope of r^{-1} at small radii but differing from the standard NFW form in its behaviour at large radii. For near spherical distributions it is natural to expand in spherical coordinates and use spherical harmonics. Equations (1) and (2) then become

$$\rho(r, \theta, \phi) = \sum_{nlm} A_{nlm} \rho_{nl}(r) Y_{lm}(\theta, \phi), \quad (7)$$

$$\Phi(r, \theta, \phi) = \sum_{nlm} A_{nlm} \Phi_{nl}(r) Y_{lm}(\theta, \phi), \quad (8)$$

where $Y_{lm}(\theta, \phi)$ are usual spherical harmonics. The zeroth order radial basis function is just the Hernquist profile

$$\rho_{000} = \frac{1}{2\pi} \frac{1}{r} \frac{1}{(1+r)^3}, \quad (9)$$

with potential

$$\Phi_{000} = -\frac{1}{1+r}, \quad (10)$$

when written in dimensionless units where $G = 1$ and the scalelength in the Hernquist form, $a = 1$. Higher order terms with $n = 0$ result from the assumption that they behave asymptotically as $r \rightarrow \infty$ as would a usual multipole expansion. To construct terms with $n \neq 0$ an additional radial function, $W_{nl}(\xi)$, is included, the form of which is found by it inserting into Poisson's equation. The transformation

$$\xi = \frac{r-1}{r+1}, \quad (11)$$

maps r from the semi-infinite range to a finite interval and simplifies the following expressions. Following the derivation from HO, the final full set of potential and density basis functions are finally found to be

$$\rho_{nl}(r) = \frac{K_{nl}}{2\pi} \frac{r^l}{r(1+r)^{2l+3}} C_n^{(2l+3/2)}(\xi) \sqrt{4\pi}, \quad (12)$$

and

$$\Phi_{nl}(r) = -\frac{r^l}{(1+r)^{2l+1}} C_n^{(2l+3/2)}(\xi) \sqrt{4\pi}, \quad (13)$$

where

$$K_{nl} = \frac{1}{2} n(n+4l+3) + (l+1)(2l+1), \quad (14)$$

and $C_n^{(2l+3/2)}(\xi)$ are the ultraspherical polynomials

(Abramowitz & Stegun 1964). The expansions can then be rewritten in purely real quantities as

$$\rho(r, \theta, \phi) = \sum_{l=0}^{\infty} \sum_{m=0}^l \sum_{n=0}^{\infty} Y_{lm}(\theta) \rho_{nl}(r) [S_{nlm} \cos m\phi + T_{nlm} \sin m\phi], \quad (15)$$

$$\Phi(r, \theta, \phi) = \sum_{l=0}^{\infty} \sum_{m=0}^l \sum_{n=0}^{\infty} Y_{lm}(\theta) \Phi_{nl}(r) [S_{nlm} \cos m\phi + T_{nlm} \sin m\phi]. \quad (16)$$

For a known density profile the expansion coefficients S_{nlm} (or T_{nlm}) can easily be obtained by multiplying both sides of equation (15) by $[Y_{lm}(\theta) \Phi_{nl}(r) \cos \phi]$ (or $[Y_{lm}(\theta) \Phi_{nl}(r) \sin \phi]$) and integrating over all space. This needs to be modified for N-body simulations where the density field is represented by discrete particles. In this case the integration over space becomes a sum over the particles, each weighted by its mass. Then the expansion coefficients are

$$\begin{pmatrix} S_{nlm} \\ T_{nlm} \end{pmatrix} = (2-\delta_{m0}) \tilde{A}_{nl} \sum_k m_k \Phi_{nl}(r_k) Y_{lm}(\theta_k) \begin{pmatrix} \cos m\phi_k \\ \sin m\phi_k \end{pmatrix}, \quad (17)$$

where

$$\tilde{A}_{nl} = -\frac{2^{8l+6}}{4\pi K_{nl}} \frac{n!(n+2l+\frac{3}{2})[\Gamma(2l+\frac{3}{2})]^2}{\Gamma(n+4l+3)}, \quad (18)$$

and r_k is the position of each particle and m_k its mass.

Once the coefficients are calculated, they can be used to evaluate equation (16) and find the potential at any location in space. Accelerations are obtained by differentiating the potential. By taking the gradient of equation (16) the accelerations can be written in spherical coordinates as

$$a_r(r, \theta, \phi) = -\sum_{l=0}^{\infty} \sum_{m=0}^l \sum_{n=0}^{\infty} Y_{lm}(\theta) \frac{d}{dr} \Phi_{nl}(r) [S_{nlm} \cos m\phi + T_{nlm} \sin m\phi], \quad (19)$$

$$a_\theta(r, \theta, \phi) = -\frac{1}{r} \sum_{l=0}^{\infty} \sum_{m=0}^l \sum_{n=0}^{\infty} \frac{dY_{lm}(\theta)}{d\theta} \Phi_{nl}(r) [S_{nlm} \cos m\phi + T_{nlm} \sin m\phi], \quad (20)$$

$$a_\phi(r, \theta, \phi) = -\frac{1}{r} \sum_{l=0}^{\infty} \sum_{m=0}^l \sum_{n=0}^{\infty} \frac{mY_{lm}(\theta)}{\sin \theta} \Phi_{nl}(r) [T_{nlm} \cos m\phi - S_{nlm} \sin m\phi]. \quad (21)$$

Both the radial and spherical harmonic basis sets are complete, so when summed from $n = 0 \rightarrow \infty$ and $l = 0 \rightarrow \infty$ the expansion converges to the exact distribution, although non-uniformly near discontinuities. However, in practice the expansions are truncated at some high order term, n_{\max} and l_{\max} . Truncated to a finite number of terms, equations (15) and (16) become

$$\rho(r, \theta, \phi) = \sum_{n=0}^{n_{\max}} \sum_{l=0}^{l_{\max}} \sum_{m=0}^l Y_{lm}(\theta) \rho_{nl}(r) [S_{nlm} \cos m\phi + T_{nlm} \sin m\phi], \quad (22)$$

$$\Phi(r, \theta, \phi) = \sum_{n=0}^{n_{\max}} \sum_{l=0}^{l_{\max}} \sum_{m=0}^l Y_{lm}(\theta) \Phi_{nl}(r) [S_{nlm} \cos m\phi + T_{nlm} \sin m\phi], \quad (23)$$

with the number of terms determining the accuracy to which the expansions reproduce the actual density distribution.

This algorithm is ideally suited to parallel computation. Each processor can independently calculate the coefficients for disjoint subsets of particles. A final summation collects together the contributions from each processor to generate the coefficients for the complete particle set. This ease of parallelism coupled with the algorithm being of $O(n)$ in the number of particles means it is ideally suited for use on huge datasets. However, the algorithm is to leading order $O(n_{\max} l_{\max}^2)$ for the number of basis terms included in the expansion and can quickly become computationally expensive if too many higher order terms are included.

2.2 Simulations

This work is based on a simulated Milky Way sized dark matter halo from the Aquarius project (Springel et al. 2008a,b; Navarro et al. 2010). The Aquarius project sample consists of six haloes of mass $\sim 10^{12} M_{\odot}$, which have each been resimulated at multiple resolutions. The simulations were performed using an improved version of GADGET (Springel et al. 2001b; Springel 2005). The cosmological model used in the simulations assumes a Λ CDM cosmogony, with parameters: $\Omega_m = 0.25$, $\Omega_{\Lambda} = 0.75$, $\sigma_8 = 0.9$, $n_s = 1$ and Hubble constant $H_0 = 73 \text{ km s}^{-1} \text{ Mpc}^{-1}$. The six haloes were selected from the set of all isolated $\sim 10^{12} M_{\odot}$ haloes from a lower resolution 900^3 -particle parent simulation of a $100h^{-1} \text{ Mpc}$ box. Isolated means that a halo had no neighbours exceeding half its mass with $1h^{-1} \text{ Mpc}$; this ensured that the haloes were not members of any massive groups or clusters. Gravitationally bound substructures orbiting within the main larger Aquarius haloes are identified using the SUBFIND algorithm (Springel et al. 2001a).

The Aquarius project haloes are ideally suited for this work as they are high-resolution simulations of single haloes, that have been carefully tested for convergence and have a large number of outputs saved at regular times. We have applied the SCF technique to two different resolution versions of the Aquarius A halo. The majority of this work is based on the higher resolution version known as Aq-A-2, while a lower resolution version, Aq-A-4, is used to check for convergence. Table 1 details the basic parameters of the simulations and haloes. There is a factor of 28 difference in the resolution of the two versions, with excellent convergence found between them. The Aq-A-2 simulation has a total of 1024 outputs, while the Aq-A-4 has only 128. For this work we have restricted ourselves to the same 128 outputs from both versions, giving one approximately every 155 Myrs at late times.

2.3 Application to Simulated Haloes

To apply the SCF method to a dark matter halo from the Aquarius simulation, we expand about the potential minimum, as identified by SUBFIND by the most bound particle. A summation over all particles is performed, once for each halo, to yield a set of coefficients that describe the halo by the given basis functions. We limit the expansions to a small number of terms, resulting in a set of coefficients much smaller in comparison to the number of dark matter parti-

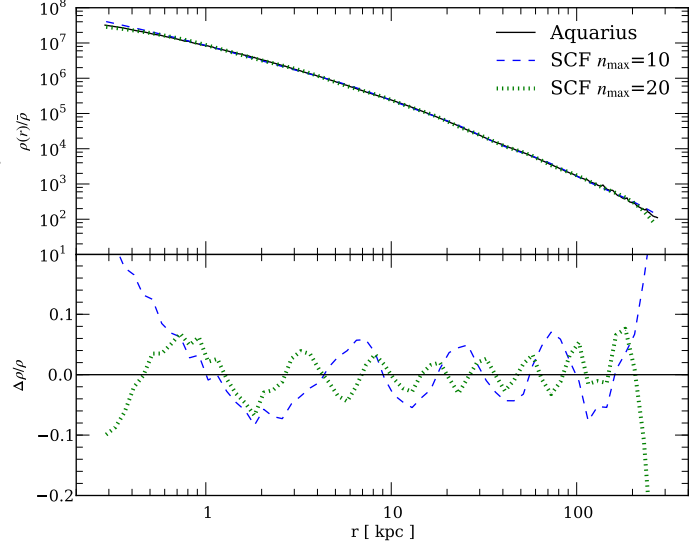


Figure 1. *Upper panel:* Spherically-averaged density profiles $\rho(r)$ of the main Aq-A-2 halo. The solid line is the profile of the actual halo from the simulation, while the dotted and dashed lines are the profiles from the SCF expansion with $n_{\max} = 10$ and $n_{\max} = 20$ respectively. *Bottom panel:* Residuals of the density profile fits, $\Delta\rho/\rho \equiv (\rho_{SCF} - \rho_{halo})/\rho_{halo}$, where ρ_{halo} is the true halo density and ρ_{SCF} denotes the SCF approximated density.

cles in the halo. This truncation of the series smooths the density and removes small-scale detail.

Only particles within 340 kpc of the halo centre, a distance larger than the halo's virial radius, are included in the coefficient summation. At greater distances, the distribution of material is more irregular and not well fitted by spherical basis functions. This sets the limit of where the halo can be well described by the SCF expansion to the internal regions where the density is smooth. While the use of a hard cut-off at the boundary imposes a discontinuity in the density profile there, we find this not to be a problem. We have tested with larger, as well as soft boundaries and find the exact choice makes little difference to our results. We choose to use a hard boundary at 340 kpc for simplicity.

Fig. 1 shows the comparison of the density profile of the main halo from the Aq-A-2 simulation, obtained by binning the simulation particles into spherical shells, with its approximation by the SCF method. The lower panel shows the residuals between the model and the data. It can be seen that over the radial range 1-100 kpc, using just eleven radial basis functions, $n_{\max} = 10$, the RMS deviation of the residuals is 4.2%, decreasing to 2.6% when twice the number of radial terms, $n_{\max} = 20$, are included. Even using just a few radial basis functions the expansion achieves a fit to within a few percent to the spherically averaged density profile of the halo, over a range where the radial density varies by over six orders of magnitude.

2.3.1 Order of Expansion

The accuracy of the SCF approximation of the halo depends on the number of terms included in the expansion, the use of more terms allows smaller spatial features to be resolved.

Halo	m_p [M_\odot]	ϵ_G [pc]	r_{200} [kpc]	M_{200} [M_\odot]	N_{200} [10^6]	V_{\max} [km/s]	r_{\max} [kpc]
Aq-A-2	1.370×10^4	66	244.84	1.842×10^{12}	134.47	208.49	28.14
Aq-A-4	3.929×10^5	342	245.70	1.838×10^{12}	4.68	209.24	28.19

Table 1. Basic parameters of the two Aquarius simulations of the A halo. m_p is the particle mass in the high-resolution region, ϵ_G is the Plummer-equivalent gravitational softening length, r_{200} is the virial radius, defined as the radius enclosing a mean overdensity 200 times the critical value, M_{200} is the mass within the virial radius, N_{200} is the total number of particles within r_{200} . Also listed is the position (r_{\max}) of the peak (V_{\max}) of the circular velocity profile.

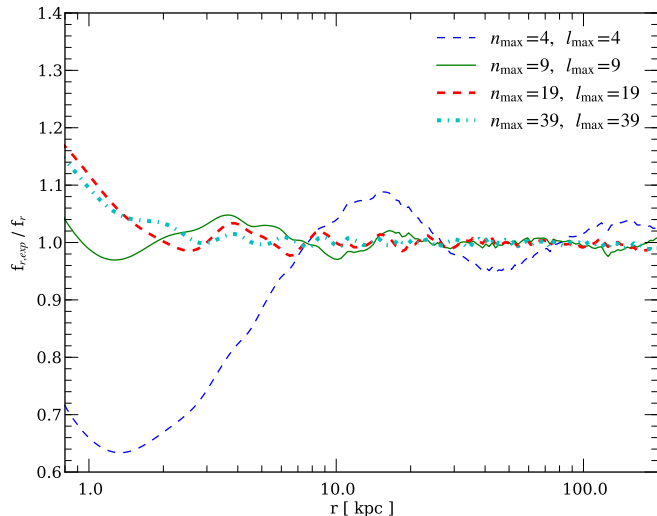


Figure 2. Radial component of the force calculated from the SCF expansion truncated at differing n_{\max} divided by the actual force calculated directly from the Aq-A-4 simulation.

The spatial resolution approximately scales inversely proportional to n_{\max} and l_{\max}^2 . To improve the spatial resolution both n_{\max} and l_{\max} need to be raised, increasing the total number of terms. The effect this has on the force can be seen in Fig. 2. Here, the radial component of the force for $n_{\max} = l_{\max} = 4, 9, 19, 39$ is compared to the force as calculated directly from the original N-body simulation.

In the central region of the haloes the radial force estimated from the expansion differs from that calculated in the simulations. The closer to the centre, the larger the disagreement. The reason for this divergence is that the density of the simulated halo has a logarithmic slope shallower than -1, while the lowest order Hernquist basis function being used to fit the simulated halo has a cusp at the centre with a slope of -1 and is not a good fit. Excluding the centre from the comparison and comparing the region between 5 and 100 kpc, it is found that doubling both n_{\max} and l_{\max} from five to ten terms each results in a big improvement, with the fractional RMS deviation falling from 4.8% to 1.3%. Doubling the number of terms again gives further gains, with expansions using 20 and 40 terms resulting in fractional RMS deviations of 0.83% and 0.46% respectively.

As the expansion is taken to increasingly higher orders, the contribution of individual terms declines. Higher order terms resolve smaller scale structure, and eventually

the very high order terms model only the shot noise from the discrete particle nature of the simulation. Following Weinberg (1996), we take the signal-to-noise on a coefficient as $S/N \equiv [S_{nlm}^2 / \text{var}(S_{nlm})]^{1/2}$, where by considering the computation of the coefficients as a Monte Carlo integration the variance can be estimated. Signal-to-noise of less than one indicates that the particle distribution does not provide significant information on the value of that coefficient. We find that terms even as high order as $n_{\max} = l_{\max} = 20$ enjoy low levels of noise and contribute to resolving the halo structure. This is not surprising as the Aq-A-2 has over 100 million particles within the virial radius, while an expansion with $n_{\max} = l_{\max} = 20$ only contains 8000 terms.

Gravity is a long-range force dominated by the large-scale distribution of material. The force on an object is therefore determined primarily by the overall distribution of mass, and resolving nearby small-scale fluctuations does not substantially improve the radial force estimate. Going to higher expansion orders is thus unnecessary, as long as we employ sufficient terms to resolve the large-scale structure. Additional terms do not provide much gain. A force accuracy of less than 1% can be achieved using $n_{\max} = l_{\max} = 20$, and is sufficient for most purposes. We use expansions to this order in the rest of this paper.

2.3.2 Choosing the Scalelength

The adopted set of basis functions contains a single free parameter corresponding to the scalelength, a , of their underlying Hernquist profile. This scalelength needs to be predetermined and chosen so that the lowest order basis function is a good fit to the halo. We find that the accuracy of the expansion when approximating the force is fairly insensitive to the exact choice of scalelength. Examination of the RMS deviation in the radial force as a function of scalelength shows that very small scalelengths give bad fits to the profile but any scalelength larger than 10 kpc is acceptable, with a minimum RMS deviation at 33 kpc. As we have already seen, the lowest order basis function is not a good fit to the halo at the origin due to a mismatch in central slopes. Reducing the scalelength does not help this.

The basis functions are primarily constrained by the region where the number of particles per radial interval is a maximum. This occurs where the logarithmic slope of the density profile is -2, which is at the scalelength for an NFW profile and at half the scalelength for a Hernquist profile. It is in this region that we desire the lowest order basis functions to fit well in order to minimise the number of terms needed in the expansion. The Aquarius A halo is very well fitted at $z = 0$ by an NFW profile with a scalelength of 15.3 kpc. It

is therefore unsurprising that the optimum scalelength for the best fit by the lowest order Hernquist basis function is found to be 33 kpc, approximately twice the the best fit NFW scalelength. Using this value obtains an average RMS deviation in the radial force between 5 and 100 kpc of 0.53%, with the force correct to within 3% down to 2 kpc. In the rest of the paper we use a scalelength of 33 kpc when modelling this halo.

2.3.3 Frame of Reference

We perform the expansion in a frame moving with the halo. Haloes are accelerated by surrounding large-scale structure. In the simulation this results in the halo having a peculiar velocity of several hundred kilometres per second, a velocity comparable to the relative motion of material within it. We wish to transform into a frame in which we can treat the halo as stationary. This will allow us to follow the relative motion of objects within a halo, such as the orbit of particles, and neglect the halo's movement through space in their equation of motion and not need to take into account the position or the velocity of the halo at intermediate times. Because of the halo's finite extent, this frame is not strictly an inertial frame, but is accelerating due to the gravitational effects of distant large-scale material. Since material within the halo experiences the same acceleration, this is only important if there are significant differential tidal forces over the scale of the halo. This is not the case, the long-range tidal force, calculated by direct summation, from distant material is less than 1% the magnitude of the internal halo force within 100 kpc of the halo centre and can be safely ignored.

In order to transform into a stationary halo frame we must define an origin that moves with the halo and remove the halo velocity. The origin of the halo frame is chosen as the halo potential minimum. This is a well defined point that follows a smooth path. The choice of the halo velocity to use for the transformation to a stationary frame is not obvious. We need to use the instantaneous halo velocity to make the correct transformation rather than the average velocity, which we could simply obtain from the motion of the potential minimum. A sensible choice is to look at the net motion of the material surrounding the potential minimum. We obtain a centre of mass velocity that should correspond to the potential minimum's velocity by selecting all particles within some bounding radius of the halo centre. Restricting ourselves to the just inner region where the halo is almost static we find that the choice of bounding radius makes little difference to the centre of mass velocity. Varying the bounding radius between 1 and 20 kpc alters the velocity by less than a kilometre per second. Including the entire halo gives a centre of mass velocity some 20 km s^{-1} different from that of the inner regions. We therefore choose to use the centre of mass velocity of the particles within 10 kpc of the halo centre as the halo velocity.

To show that this is a valid choice we compare the orbits of particles integrated within the expansion to the orbits the same particles took within the original simulation. The next section describes this in detail. Through this procedure we have found that for a set of particle orbits there is an optimal velocity for the halo frame in which to integrate particle orbits in order to match their equivalent orbits from the Aquarius simulation. This velocity can be found through a

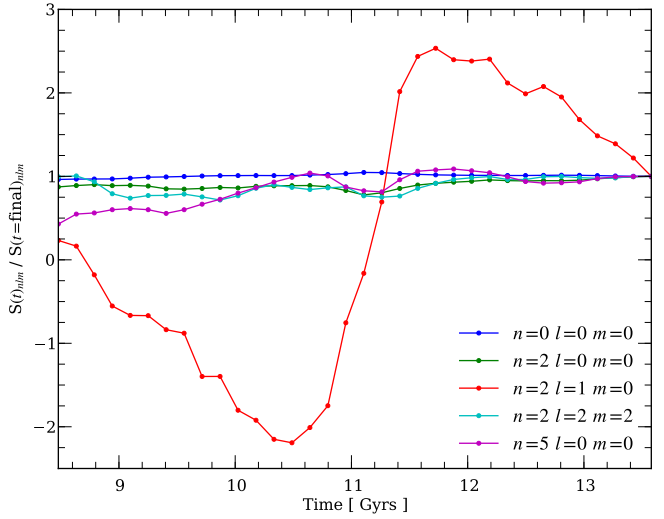


Figure 3. The variation of low order coefficients as a function of time for the last 5 Gyrs of the Aq-A-2 halo evolution.

minimisation scheme, in which we attempt to minimise the difference in their final position compared to their position in the original simulation. The optimum velocity depends on the set of orbits considered, but the velocity only varies within a few kilometres per second between cases. This allows us to define a window of several kilometres per second in which we find that any choice of velocity for the halo frame works satisfactorily. Choosing a different velocity within this window changes the results by only a percent or two. Not only does this show that an approximately stationary frame does exist, we also find that the centre of mass velocity that we chose earlier lies within this window. This is true for both the Aquarius A and B halo and demonstrates this to be a valid choice for the halo frame, especially as it can be easily determined in advance, whereas the optimum velocity for a particular case can be only located retrospectively.

2.3.4 Time Variation

Due to the fact that such a large amount of data is generated, the output of N-body simulations is usually recorded only at a few snapshots. Between these snapshots information on the exact evolution of the halo is lost. However, it is usually sufficient to use simple interpolation to approximate it. The SCF technique is ideal for this because at each snapshot a new set of coefficients are calculated to describe the halo at that time. An approximation to the state of the halo at any intermediate time can be recovered by linearly interpolating the coefficient of each basis function between the directly preceding and following snapshots.

Fig. 3 illustrates the variation in a selection of low order coefficients over the last 5 Gyrs of the Aq-A-2 halo's growth, with a time resolution set by the snapshot spacing, of 155 Myrs. The coefficient of the lowest order basis function varies very little, initially showing a slight increase until 11 Gyrs, followed by a slight decline. The variation corresponds to the slight fluctuation in mass of the inner ~ 100 kpc of the halo. The higher order coefficients have

greater variation. The fluctuations on short timescales, of the order of the time spacing of the snapshots, are generally small, while the larger, more important, variations, such as the oscillation in the $n = 2, l = 1, m = 0$ coefficient, occur on longer timescales. The time spacing we use is sufficient to capture large-scale changes in halo structure. Smaller quicker changes, such as those from substructure, may be missed but this does not matter as these are not spatially resolved by the expansion anyway.

3 RESIMULATING AQUARIUS

Once we have obtained a time-varying set of coefficients for an SCF expansion approximation to an Aquarius halo potential and density, it is straightforward to use this to integrate orbits of test particles within the evolving halo potential. In order to test the accuracy of the SCF expansion method, we attempt to reproduce the orbits and properties of existing objects already present in the Aquarius simulations. Based on the findings of the previous section we use an SCF potential expansion including terms up to order $n_{\max} = 20$ and $l_{\max} = 20$, with a fixed scalelength of 33 kpc and summed over all particles within 340 kpc of the halo centre, to approximate Aq-A-2 halo. A set of coefficients is generated for each snapshot, approximately every 155 Myrs.

3.1 Integrating Orbits

3.1.1 Single Particles

We start by considering the orbits of single particles. Ideally, if the potential is approximated accurately, test particles placed in the evolving halo potential will behave in the same manner as particles in the original simulation. This should be the case as long as the particles are not bound to any subhalo, since we are not attempting to resolve this level of detail. Therefore, by setting up a test particle with initial conditions matching the instantaneous state of a simulation particle and integrating the orbit within the SCF halo approximation, a comparison can be made between the path that the simulation particle actually followed and the one recreated using the SCF method. Differences in the orbital path or properties provide a guide to the accuracy of the SCF approximation.

We randomly select 10,000 particles from the Aq-A-2 simulation that are within 140 kpc of the halo centre at a redshift $z = 0.5$ and extract their orbits by tracking their positions through successive snapshots. Non-interacting particles, placed at the same initial position and with the same velocity as the selected particles, are then integrated within an SCF potential expansion of the same halo for 5 Gyr, using a simple drift-kick-drift leapfrog integrator with a fixed time step of 1 Myr. A shorter time step has no significant effect on the results.

Fig. 4 shows an example of an orbit extracted from the Aquarius Aq-A-4 simulation of a particle randomly selected from the set of particles with orbits confined to the central 15 kpc of the halo. The orbit is compared with one integrated for 1 Gyr in the SCF potential. The recreated orbit closely matches the actual particle path but over time the orbits diverge. By the end of the integration there is

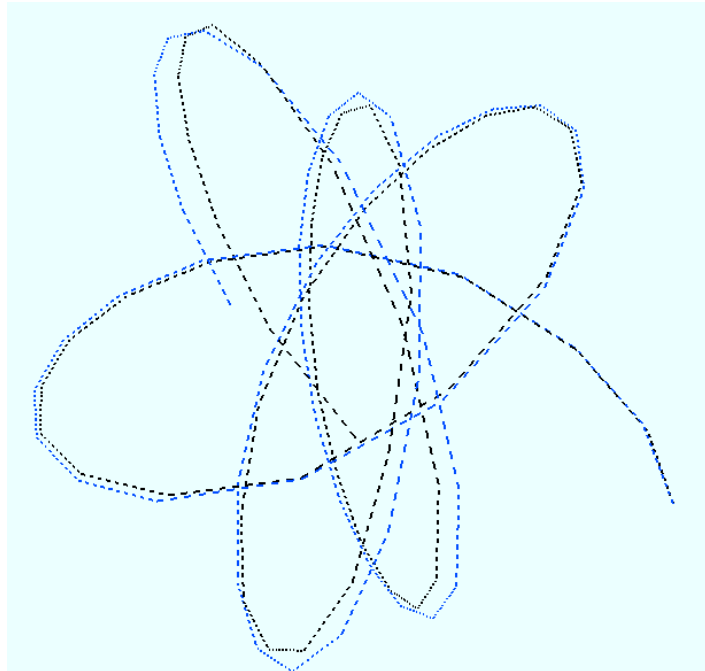


Figure 4. The orbit of a single particle in the Aq-A-4 simulation. The blue line shows the result of using the SCF approximation. The black line shows the actual path of the same particle followed through the Aquarius simulation. The particle positions were recorded only at limited points which have been joined by straight lines. Both paths start from the same point on the right and are integrated for 1 Gyr.

some displacement between the final positions. While the orbit shape is well reproduced, the progress of the particles along their orbits are slightly out of phase. This discrepancy was introduced during the 3rd apocentre passage, when the resimulated particle took a slightly wider orbit so that it subsequently lags behind the actual particle. An increasing divergence in paths is not unexpected as once a particle has even slightly different phase space coordinates it will subsequently follow an increasingly different orbit. The energy of the two particles is matched to within 1.3% throughout the entire orbit, while the difference in the magnitude of the angular momentum is greatest at the 3rd apocentre when it is 17%.

The final energy and angular momentum are more indicative of differences in orbits than final position. Position is an instantaneous phase space coordinate that rapidly varies along an orbit and absolute differences in position are dependent on a particle's current radial distance from the halo centre. In contrast, energy and angular momentum, although not integrals of the motion since the potential is both time-varying and non-spherical, vary slowly along the orbit and are altered by accumulated changes. The differences in the final energy and angular momentum are therefore more dependent on the entire orbital history than the difference in final position and provide a better way to compare orbits.

The results for the relative differences in energy and angular momentum for the complete sample of 10,000 particles can be seen in Fig. 5. The relative final energy is matched to within 20% by 95% of orbits, but the angular momentum is matched to within this limit by only 40% of orbits.

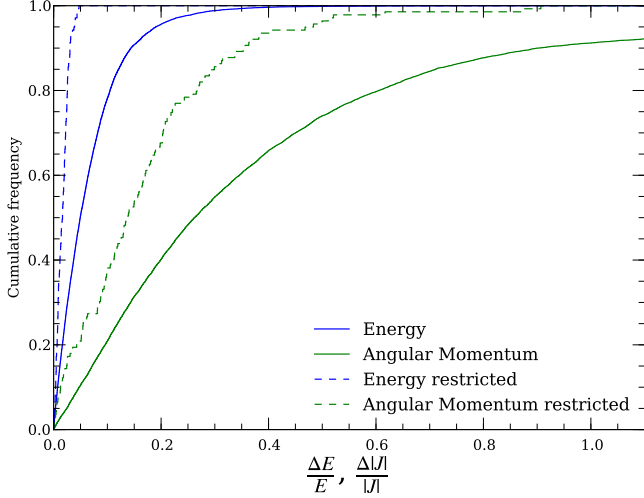


Figure 5. Cumulative distribution of the fractional differences in the final energy and angular momentum of particle orbits. Test particles are integrated with an SCF expansion for 5 Gyrs and their final energy and angular momentum compared to the orbits the same particles followed in the original Aquarius simulation. The solid lines show the results for ten thousand randomly chosen particles lying within 140 kpc at $z = 0.5$, while the dashed lines are for a smaller subset of 140 particles on near circular orbits, with $3 \text{ kpc} \leq r \leq 20 \text{ kpc}$.

We have checked that energy is conserved to better than 0.1 percent for orbits within a static SCF potential, confirming that the changes in energy are not due to the numerical integration. The reason why the angular momentum is less well matched is that changes in energy are caused by the time variation of the potential, a slowly varying quantity, while changes in angular momentum are introduced by the non-spherical nature of the halo. The angular momentum varies more rapidly with the changing spatial position along an orbit and any slight phase mismatch in orbital positions can result in a large difference in the instantaneous angular momentum. Thus, we find that angular momentum is much more variable and that the width in the distribution of the final to initial angular momentum is almost nine times that of the width of the final to initial energy. It is therefore not surprising that final energy is better matched than final angular momentum.

Some of the test particles' orbits are significantly different to their Aquarius counterparts; they initially match the actual orbits but suddenly diverge and follow significantly different paths. This occurs primarily for particles with low angular momentum on nearly radial orbits. The pericentric passages of these orbits are very close to the centre of the halo. At the centre even slight differences in orbits cause particles to be scattered in radically different directions. As well as the centre, which is responsible for the majority of these scatterings, encounters with subhaloes can have a similar effect. Particles can either be scattered off subhaloes or become bound to them. To resolve a subhalo 1 kpc in size and 50 kpc from the centre would require at least an expansion with $n_{\text{max}} = 150$ and $l_{\text{max}} = 150$, over 3 million terms.

Even though individual orbits integrated in the SCF

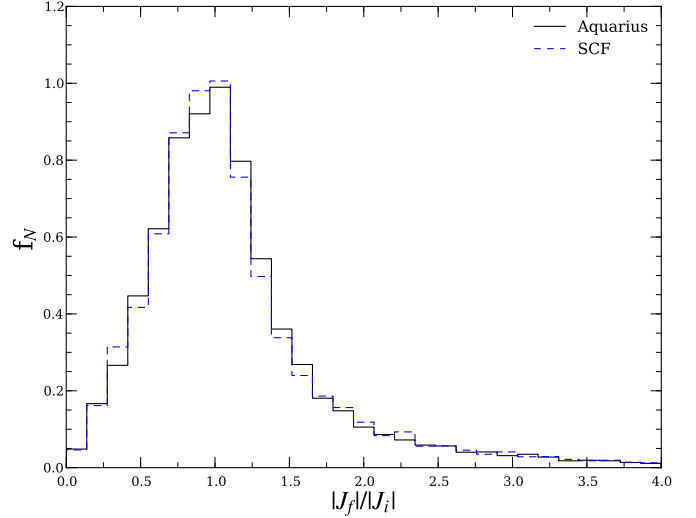


Figure 6. The distribution of the magnitude of the final angular momentum of a test particle compared to its initial angular momentum for the 10,000 test particles.

approximation do not always match their counterparts, the overall distribution of changes in the energy and in the magnitude of the angular momentum are well reproduced. This can be seen in Fig. 6, the ratio of final to initial angular momentum. The very similar distributions suggest that while individual orbits may be scattered differently, there is no systematic difference in orbits integrated in the SCF approximation and those found in the Aquarius simulation. We find an even better match for energy.

Orbits confined near to the centre of the parent halo are better matched than ones with larger apocentric distances. This is a consequence of both the fact that the basis functions used in the SCF approximation have lower spatial resolution at larger radii and thus structure is not resolved as clearly in the outer regions, and the fact that the halo is smoother towards the centre than nearer its virial radius. This suggests that the SCF method works best for describing the smooth inner parts of the halo. To resolve the full outer structure of a halo would require a very large number of basis functions.

Restricting our attention to particles confined to a region near the centre of between 3 kpc and 20 kpc, where the SCF expansion is very successful, selects particles on near circular orbits. When we consider the differences in energy and angular momentum for these orbits (dashed lines in Fig. 5), we find that the SCF approximation is particularly good. The relative difference in the final energy is within 4.7% for all orbits and 67.5% of orbits match the angular momentum within 20%, 1.6 times as many as for the complete sample. Orbits in this region are of particular interest when considering galactic disks.

3.1.2 Subhaloes

Having demonstrated that it is possible to successfully recreate single particle orbits, we now turn our attention to the same question for subhaloes. These are large, gravitationally bound, extended bodies undergoing tidal evolution as

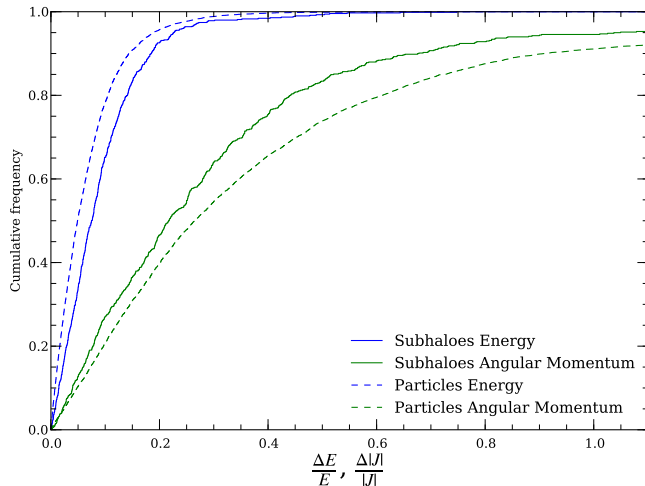


Figure 7. Cumulative distribution of the fractional differences in the final energy and angular momentum of recreated subhalo orbits. Subhaloes are integrated as extended bodies within an SCF expansion for 5 Gyrs and their final energy and angular momentum compared to the orbits of the same subhaloes tracked in the original Aquarius simulation. The solid line shows the results for the subhaloes. For comparison the dashed lines are for similarly selected particles.

they orbit within the parent halo. We compare the orbits integrated within the SCF expansion potentials when the subhaloes are treated as both point masses and extended objects, to the orbits of subhaloes from the Aquarius simulation. In a similar manner to the single particles, subhaloes are selected from the Aquarius simulation and tracked through successive snapshots to identify their orbits, which we then attempt to recreate using the SCF approximation.

To model a subhalo as an extended body, we select the subhalo from the Aquarius simulation and identify all the particles that SUBFIND assigns to it. The same particles are extracted from subsequent snapshots and SUBFIND is run on just this particle set to calculate those that are still gravitationally bound. This results in a complete orbital path and record of the subhalo’s evolutionary history. A copy of the initial subhalo is then integrated in an SCF expansion of the potential. The subhalo is composed of multiple particles that are allowed to interact gravitationally with each other. This has been done using a version of GADGET modified to allow an additional external potential from an SCF expansion.

The contribution to the potential from a subhalo needs to be removed from the SCF expansion of the potential that is used to resimulate its orbit. Not excluding the self-contribution would lead to a double counting of the subhalo, because the gravitational effects of the subhalo are already included in the potential expansion and double counting would generate an unrealistic self-attraction to the counterpart resimulated with the SCF expansion. Since the coefficients are just linear sums it is easy to remove the contribution from the subhalo by separately calculating the coefficients of just the subhalo particles from the original simulation and subtracting them from the total coefficients.

From the Aq-A-2 simulation we selected all 1507 sub-

haloes with 100 or more particles that are within 90 kpc of the centre of the parent halo at $z = 0.5$. Their orbits are then followed using the modified GADGET for 5 Gyrs in the same SCF expansion as used for single particle orbits. One limitation of the SCF technique for subhaloes is that it ignores dynamical friction. However, an estimate of the dynamical friction on a subhalo based on the Chandrasekhar model (Chandrasekhar 1943) shows that it is negligible for the majority of subhaloes and only really important for the most massive ones. Since the majority of our samples are small subhaloes of mass $\sim 10^6 M_\odot$, dynamical friction can therefore be discounted as a significant source of error in reproducing subhalo orbits. Dynamical friction could be added to the equation of motion but would require an estimate of a subhalo’s size and mass. This information is not available until the simulation is post-processed by SUBFIND or unless some subhalo evolutionary model is assumed.

The results for subhaloes’ final energies and angular momenta are similar to those for single particles; most orbits are very well matched while others are not. Fig. 7 shows the relative differences in energy and angular momentum for both subhaloes and particles. There is a slight difference between the cumulative distributions of subhaloes and particles but this can be explained by the two having differing spatial distributions within the halo, rather than by any difference in the way subhalo orbits are treated compared to particles. In fact, we find that there is very little difference between the orbits of subhaloes when treated as point masses and when treated as extended bodies. Over 87% of the subhaloes have a difference of less than 10% in their final angular momentum in the two cases. This suggests that the extended nature of the subhalo has very little effect on its motion and even though mass is being continuously stripped from the subhalo, forming leading and trailing streams, these do not have a significant effect on its orbit.

Particle orbits integrated in the SCF approximation match the final energy better while subhalo orbits match the final angular momentum better. Particles are more centrally concentrated than subhaloes. The centre of a dark matter halo is dynamically older and therefore more relaxed and stable than the outer regions, so there is less time variation of the potential. This conserves energy along orbits near the centre better than along orbits that pass further out. For angular momentum the opposite is true, the central regions of a halo are more triaxial, with the halo becoming increasingly spherical with increasing radius, leading to greater variation in angular momentum along an orbit near the centre. For the more centrally concentrated orbits of particles the SCF approximation is therefore better at reproducing the mildly varying energy but worse at reproducing the strongly varying angular momentum.

The majority of cases where the Aquarius subhalo orbits and the resimulated orbits dramatically differ are again the result of scattering events. Subhaloes are scattered from the centre of the parent halo, in the same way as particles, and any slight differences in the orbits are greatly amplified during the pericentric passage. However, as well as scattering off the centre, subhalo-subhalo scattering events are found to be more frequent than for single particles. When two subhaloes strongly interact, the orbit of at least one of the pair can be completely changed. In particular, a large subhalo merging into the parent halo will scatter any small

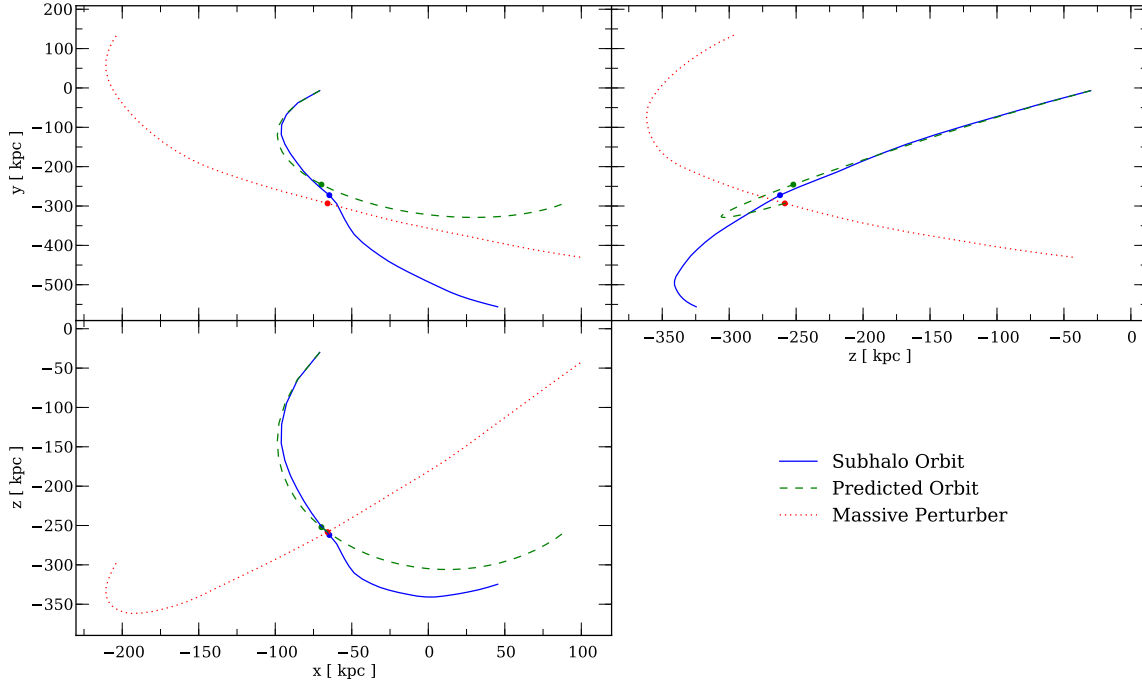


Figure 8. Three orthogonal projections showing the orbit of a subhalo and how it is affected by a close encounter with a massive subhalo. The green dashed line shows the smooth orbit the subhalo was predicted to follow by integration in an SCF expansion. The blue solid line is the orbit the subhalo actually followed in the Aquarius simulation. The red dotted line is the orbit of the $1.6 \times 10^{10} M_{\odot}$ subhalo that scatters the small subhalo. The dots on the lines indicate the point of closest approach.

subhaloes it passes as it falls in. The dramatic effect subhalo scattering can have on an orbit is illustrated in Fig. 8. Here a subhalo of mass $3 \times 10^6 M_{\odot}$, initially located at 70 kpc at $z = 0.5$ from the centre of the Aquarius parent halo, follows an orbit that takes it to the outer edge of the parent halo. At this point, just prior to apocentre, the subhalo passes within 20 kpc of a massive $1.6 \times 10^{10} M_{\odot}$ subhalo and is scattered. Rather than falling back into the parent halo as originally destined to do, the subhalo is thrown outwards on to a larger, higher energy orbit but still remains bound to the Aquarius halo. These subhalo-subhalo interactions are not well reproduced in the subhalo simulations using the SCF approximation since, while contributions to the potential from subhaloes are included, these are not well enough resolved with the number of basis functions we use to model scattering. Instead, the potential from subhaloes is blurred out.

3.2 Subhalo Evolution

As subhaloes orbit within their parent halo they are tidally stripped and shocked, losing mass and decreasing in size. Exactly how subhaloes evolve and their final fate is a problem that has been extensively studied (Peñarrubia & Benson 2005; Angulo et al. 2009). The ability to model subhaloes as extended bodies allows a comparison between their structural evolution in a resimulation and in the Aquarius simulation. We resimulate subhaloes in three different potential

expansions corresponding to differing levels of sophistication. The simplest is a fixed, spherically symmetric Hernquist potential, an example of an analytical potential that is commonly used to represent dark matter haloes in simulations (Adams & Bloch 2005; Bullock & Johnston 2005). The second is an SCF expansion that includes only radial basis functions to obtain the correct radial mass distribution, but with no information about the shape of the halo. The final potential is a full SCF expansion including both radial and angular terms. We use the three different potentials in order to assess the difference between the evolution of subhaloes using the commonly employed method with a static simple potential and the effect of using a full time-varying triaxial approximation.

The parameters for the Hernquist potential are chosen so that it matches the lowest order basis function from the expansion of the halo at $z = 0$. It has a scalelength of 33 kpc and a total mass of $2 \times 10^{12} M_{\odot}$. This is a good fit to the halo at the final time but overestimates the mass at earlier times. The second potential (SCF_R), using only radial terms, has $n_{\max} = 20$ and $l_{\max} = 0$, with a scalelength of 33 kpc and has time-varying coefficients. The full potential (SCF₂₀), uses the default parameters, so it has $n_{\max} = 20$ and $l_{\max} = 20$, is also time-varying and has a scalelength of 33 kpc. Again, we exclude the contribution to the SCF potential from the resimulated subhaloes.

3.2.1 A Single Subhalo

We start by focusing on a single subhalo to illustrate the technique in more detail. This subhalo has been selected from the Aq-A-2 simulation and contains 13120 particles, with a total mass of $1.8 \times 10^8 M_\odot$. The subhalo was selected at redshift $z = 0.5$, and resimulated for 5 Gyrs, with output snapshots every 155 Myrs. It is compared to the same subhalo extracted at the same times from the Aq-A-2 simulation.

Fig. 9 shows the radial distance of the subhalo from the centre of the potential and three main structural properties that describe the state of a subhalo: the mass, the maximum circular velocity and the half-mass radius. The properties of the subhaloes in the two simplest methods, the Hernquist potential and the SCF_R , immediately diverge from that of the Aquarius simulation, as a consequence of the fact that they follow different orbits, as may be seen in the top panel. These different orbits cause the subhalo to experience different tidal stripping and, at pericentre, different amounts of tidal shocking, resulting in incorrect estimates of the structural properties. In the SCF_{20} resimulation the subhalo follows an orbit very closely matching the actual subhalo's orbit for the first 2.5 Gyrs, until, following the first pericentric passage, the orbits begin to diverge. Subsequently, the Aquarius subhalo reaches a greater apocentric distance and falls back in slightly later. Following this, near the halo centre, the small differences in the paths are sufficiently large that during the second passage the SCF_{20} resimulated subhalo and the original Aquarius subhalo pass the centre on opposite sides and depart in different radial directions.

During the initial period while the orbit of the subhalo in the SCF_{20} resimulation closely follows the fiducial Aquarius orbit, the subhalo properties, the mass, half-mass radius and maximum circular velocity, are reproduced extremely well. The subhalo is stripped and distorted in the same manner as in the Aquarius simulation. The subhalo continuously loses mass as it orbits within the parent halo, with sudden and large decreases during pericentric passages. Similarly, the maximum circular velocity, which is determined by the mass in the inner regions of the subhalo, is unaffected as mass is stripped from the outer edge. It is only when the subhalo makes a close approach to the parent halo centre and is tidally shocked and subject to maximum tidal stripping that the internal structure of the subhalo is notably changed. This behaviour is seen both in the Aquarius simulation and the SCF_{20} resimulation and indicates that the important gravitational mechanisms - tidal stripping and shocking, responsible for the evolution of a subhalo - are equivalently modelled by the full SCF expansion as they are in the full simulation.

An instantaneous picture of the subhalo during its second apocentre can be seen in Fig. 10. Rather than comparing the subhalo at the same time, it is fairer to compare it at the same position along the orbit as this removes any difference in orbital phase. The resimulated subhalo in the SCF_{20} potential is strikingly similar to the original Aquarius subhalo. It is close to the correct position, at the correct time and has very similar tidal tails. This similarity includes the small perpendicular protrusion to the left of the subhalo, which is a result of the end of the trailing tidal tail being

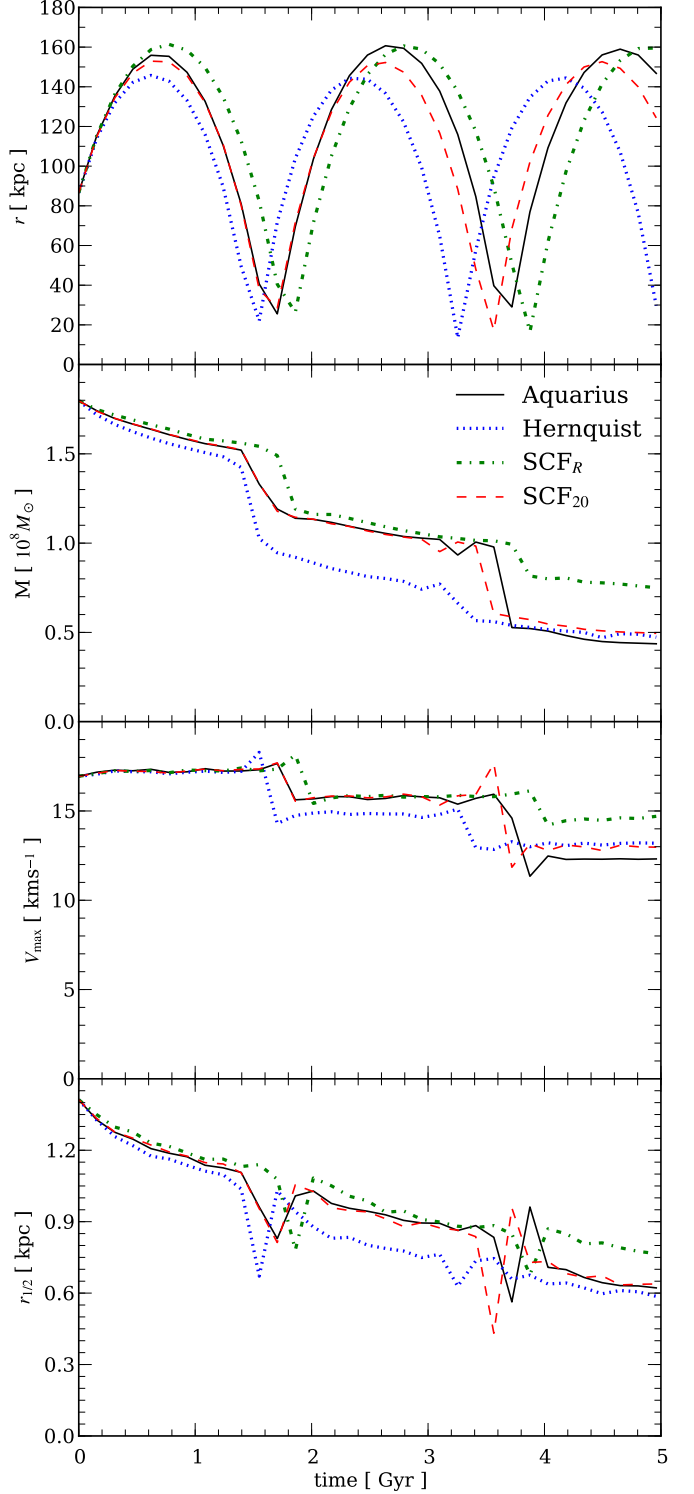


Figure 9. Comparison between the properties of different versions of the same subhalo. The full Aquarius Aq-A-2 is represented by the black line. The other lines show resimulations of the subhalo in three differing potentials. *Upper panel:* the distance of the subhalo from the centre of the parent halo. *Upper middle panel:* the mass of the subhalo. *Lower middle panel:* the maximum circular velocity. *Bottom panel:* the half-mass radius.

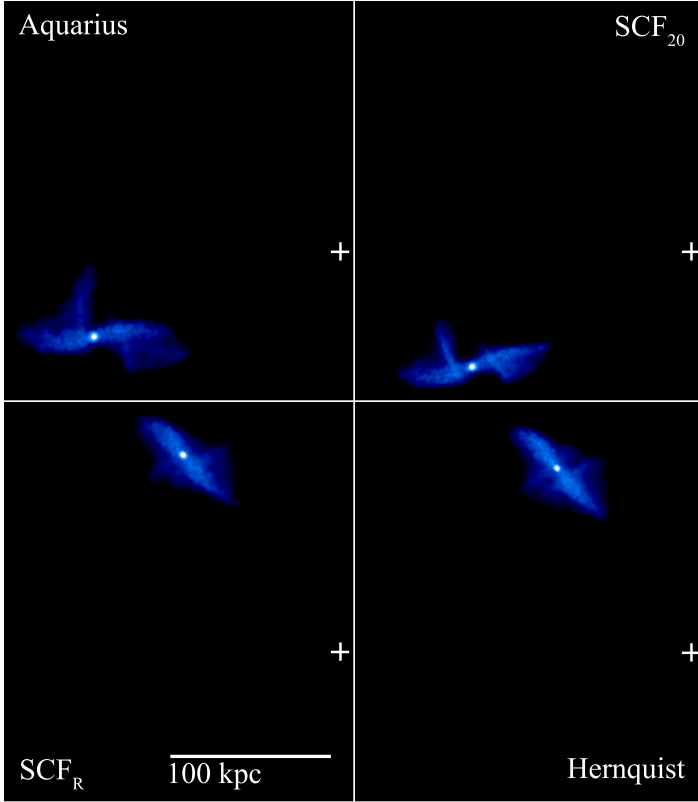


Figure 10. A projection of the smoothed density of a single subhalo resimulated in various different potential approximations at the subhalo’s second apocentre. The subhalo reaches second apocentre at different times in the resimulations. The cross marks the centre of the parent halo in each case. *Upper left panel:* the subhalo at 2.6 Gyrs in the original Aquarius simulation. *Upper right panel:* the subhalo at 2.6 Gyrs in the full SCF₂₀ potential expansion. *Lower left panel:* the subhalo at 2.8 Gyrs in the SCF_R potential expansion. *Lower right panel:* at 2.3 Gyrs in a static Hernquist potential.

broken off during the apocentric turn-around. In contrast, there is little resemblance between the subhalo in either the Hernquist or the SCF_R resimulation and the Aquarius original, though there is a strong resemblance with each other. Both potentials are spherical, confining the subhalo to orbit in a plane, and thus the two potentials generate similarly shaped orbits. However, there is a large phase difference between the two. The Hernquist subhalo reaches the second apocentre 290 Myrs before the Aquarius subhalo, while the SCF_R reaches second apocentre 140 Myrs after the Aquarius subhalo.

The final values of the mass, maximum circular velocity and half-mass radius, are similar in the Hernquist and SCF₂₀ resimulations but this is more a coincidence than the result of the subhalo having the correct evolution in the Hernquist potential. While not completely correct, the evolution of the subhalo is much closer to the real case when the full SCF expansion is used than when the simplified potentials are used. This suggests that both the radial mass distribution and the angular shape of the halo are important for reproducing correct orbits, which is a prerequisite to achieve similar evolution.

3.2.2 Subhalo Population

To assess whether the evolutionary mechanisms on subhaloes are the same even though the orbits may not exactly match, we now consider a population of subhaloes and look at the statistical match between a set of Aquarius reference subhaloes and resimulations of them in the three potentials. From the Aq-A-2 simulation we again use the set of selected subhaloes with 100 or more particles that are within 90 kpc of centre of the parent halo at $z = 0.5$. The particles belonging to these subhaloes are then tracked forward in time to follow the subhaloes’ evolution in the full simulation.

Fig. 11 shows the population distribution of the three main structural properties of subhaloes: the mass, the half-mass radius, and the maximum circular velocity. The distribution of the ratios of the final to the initial property has been used to remove the influence of the property distribution and allow an easier comparison of the actual evolution that the subhaloes undergo during 5 Gyrs. The distribution of mass ratios shows how much stripping the subhaloes experience. Nearly all subhaloes in the Aquarius simulation lose mass over the 5 Gyrs but a small fraction gain mass. The gain in mass can be explained by inter-subhalo mergers, where two or more subhaloes join to form a larger subhalo. The SCF resimulations and the Aquarius simulation have the same small fraction of subhaloes undergoing this mass increase; they have similar distributions of mass ratios, with the same wide spread and a peak that occurs at 0.65. Only the Hernquist potential shows significant difference.

Similarly, the half-mass radius distribution is well matched by the resimulations, except again by the Hernquist potential which is slightly shifted to smaller sizes. Even though subhaloes generally lose mass, a small proportion grow in size. This can occur when a subhalo passes pericentre and is tidally shocked by the rapidly changing potential field, thus increasing its internal energy and resulting in an increase in size. This occurs in both the Aquarius simulations and SCF resimulations. The maximum circular velocity distribution is very slightly smaller in all the resimulations, with the largest discrepancy again for the Hernquist population. The primary reasons why the results from the Hernquist resimulation are so different from the other two are the assumption of a static potential of fixed mass throughout the whole simulation, which overestimates the actual mass of the Aquarius halo at early times, and the fact that a Hernquist potential gives the incorrect tidal radius for subhaloes. The tidal radius is the distance from the centre of a subhalo at which the gravitational tidal pull from the parent halo is equal to the pull from the subhalo itself. Material outside of this radius is stripped from the subhalo and becomes part of the parent halo. We find that the Hernquist potential leads to underestimates of the tidal radius for subhaloes that are between 30 and 200 kpc from the centre of the parent halo and to overestimates outside this range. The subhaloes therefore experience a different rate of stripping over the course of their orbits than they do in the original simulation and the other cases.

Since the SCF_R expansion achieves an equally good match to the Aquarius simulation as the full SCF expansion that also includes the angular terms, we conclude that the shape of the potential is unimportant for reproducing the structural evolution of the subhalo population in a statisiti-

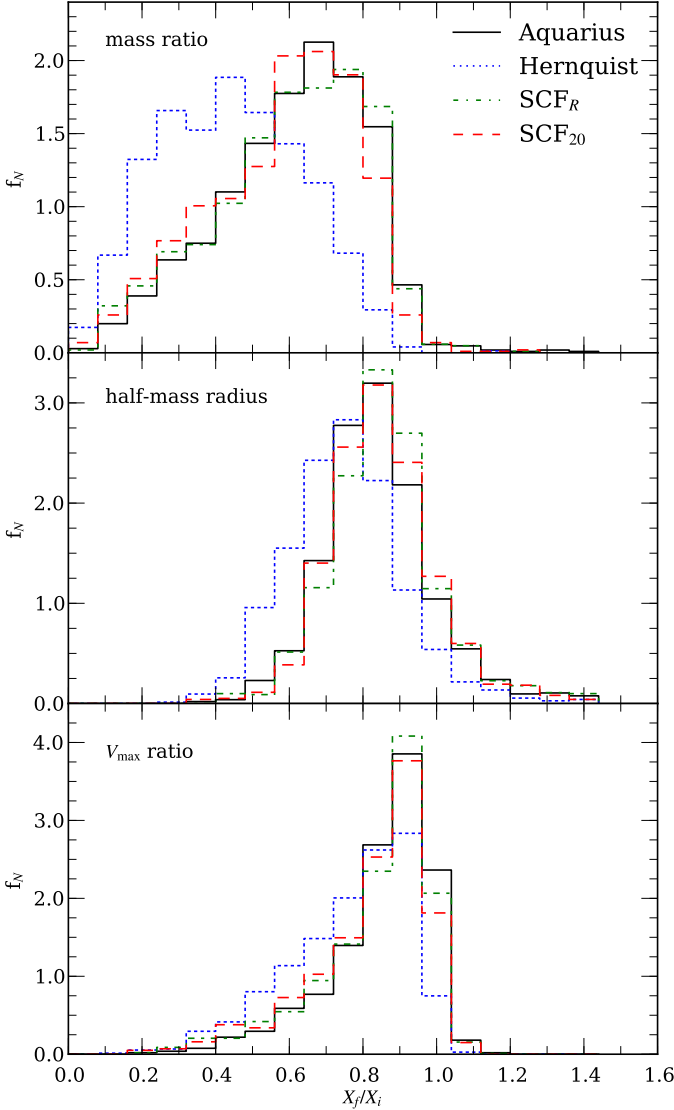


Figure 11. The distribution of X final over X initial for a selected Aquarius subhalo population for three different physical properties. The black line shows the actual distribution that occurred in the original Aquarius simulation while the other colours correspond to the different resimulations. For each subhalo, the ratio is the given property at $z = 0$ compared to its initial value at $z = 0.5$. *Upper panel:* the distribution of final to initial mass ratios. *Middle panel:* the distribution of final and initial half-mass radii. *Bottom panel:* the distribution of final to initial maximum circular velocities.

cal sense; only the radial mass distribution needs to be correctly reproduced. The stripping of mass from a subhalo is controlled by the tidal radius of the subhalo, so reproducing this property correctly ensures the correct overall evolution. This can be done by matching the radial mass distribution, which is easily achieved with a small number of basis functions. In order to obtain similar evolution on a individual subhalo basis, the orbits need to be well matched, which does require the angular distribution and the full SCF expansion.

4 APPLICATION

Having shown that the orbits, as well as the subhalo evolution, are similar in an SCF expansion and in the original simulation, we now demonstrate how the SCF technique can be used to go beyond the original simulation. The introduction of new objects into the halo that were not present in the original simulation, allows us to investigate the reaction of these objects as if they had evolved in a cosmologically realistic potential. They are unable to induce a back reaction on the halo, but we are the method is appropriate for studying light objects that would have had little effect on the halo. This can be achieved at a much lower cost than re-running a complete simulation and is more realistic than assuming a fixed analytical profile, such as a Hernquist profile.

4.1 Increasing Subhalo Resolution

We now illustrate the technique of placing new, additional subhaloes into the potential and simulating them at much higher resolution. As a test, a subhalo is constructed to be similar to the subhaloes found in the simulations, with an NFW density profile

$$\rho(r) = \frac{\rho_0}{\left(\frac{r}{r_s}\right) \left(1 + \frac{r}{r_s}\right)^2}, \quad (24)$$

with $\rho_0 = 8 \times 10^7 M_\odot \text{kpc}^{-3}$ and $r_s = 0.27 \text{ kpc}$, and an isotropic velocity distribution. The subhalo is injected into the SCF potential approximation of the Aq-A-2 halo. To create equilibrium N -body halo realisations, we have used the algorithm described in Kazantzidis et al. (2004) based on sampling the phase-space distribution function to generate the subhalo. Since the mass of an object with an NFW profile does not converge with radius, we truncate the subhalo at the virial radius using an exponential cut-off with a decay length set to ten times the virial radius. This ensures the subhalo has a finite mass.

We generate the initial subhalo at two resolutions. The first, lower resolution version consists of 6000 particles with masses of $1.4 \times 10^4 M_\odot$, the same particle mass as the Aq-A-2 simulation. The second version contains 10^6 particles, a resolution 170 times higher, with individual particles masses of just $82 M_\odot$. Since the subhalo is small, with a SUBFIND mass of $5 \times 10^7 M_\odot$, the absence of dynamical friction should not be significant. The subhalo is placed 190 kpc from the halo centre, approximately at the virial radius of the parent halo, where it will be just entering into the main halo and will not yet have been significantly stripped. The subhalo is simulated from $z = 0.5$ for 5 Gyrs.

The orbits of the two different resolution versions of the subhalo are virtually identical. This is not unexpected, as we have already found that subhaloes orbit as point masses regardless of their extended nature. The changes in the properties of the subhalo over the 5 Gyr simulation are shown in Fig. 12. Here we compare the evolution of the mass, maximum circular velocity and half-mass radius between the low and high resolution simulations. While both realisations of the subhalo are sampled from identical NFW profiles, the initial SUBFIND mass is slightly higher for the low resolution version. Later mass estimates agree, suggesting that in both cases the subhalo was stripped to the same tidal radius, and the same material was lost regardless of whether

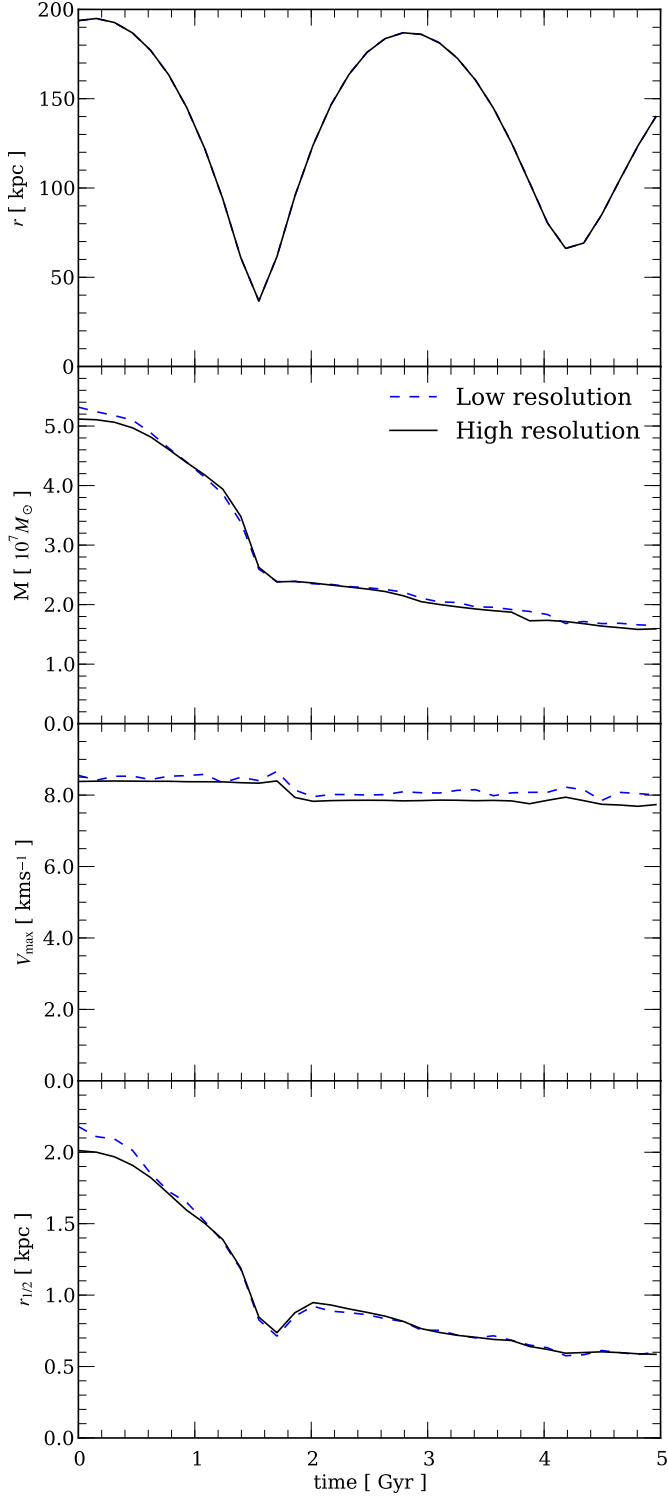


Figure 12. Comparison between the properties given by SUBFIND for a subhalo simulated for 5 Gyrs at two resolutions in the SCF expansion. *Upper panel:* the distance of the subhalo from the centre of the parent halo. *Upper middle panel:* the mass of the subhalo. *Lower middle panel:* the maximum circular velocity. *Bottom panel:* the half-mass radius.

SUBFIND had initially associated it with the subhalo or not.

The maximum circular velocities again are very slightly different, but the higher resolution version has a smoother evolution since it is less affected by noise from the discrete particle nature of the subhalo. The half-mass radius has the same initial discrepancy as the mass, but again agrees at later times, with both versions undergoing the same compression of the subhalo during the first pericentric passage. Overall there is excellent convergence between the two resolutions and it is clearly demonstrated that the structural evolution is independent of the resolution of the subhalo as expected.

Apart from studying the subhalo we can compare the fate of the material that is stripped from it and forms streams. There is both a leading stream and a trailing stream, containing material that is no longer bound to the subhalo but continues to follow similar orbits. These streams match in the high and low resolution simulations but are much clearer and can be traced much further in the high resolution version. Sections of the streams containing a few tens of particles in the low resolution version are now populated with thousands of particles in the high resolution simulation. Features that had been only hinted at are clearly defined in the high resolution simulation. Especially clear are the caustics of the streams which can be seen in Fig. 13. Another feature that is not resolved in the low-resolution simulation but is clearly visible in the high-resolution version is the bifurcation into two separate arms of the leading tidal tail, the one above the subhalo in Fig. 13.

The SCF method allows us to simulate a subhalo at different resolutions, with clear convergence between the two cases we have examined. By focusing computing resources on just the subhalo and using an approximation to the potential of the larger parent halo, we have been able to reach an unprecedentedly high resolution, using a particle mass of a few tens of solar masses and resolved tidal streams much further and in a much sharper way than has been previously achieved. The low-resolution simulation required only 15 cpu hours¹ and the high-resolution subhalo only 2700 cpu hours. This is small compared to the Aquarius A level 2 simulation, which has equivalent resolution to the low-resolution subhalo and which took of order $\sim 150,000$ cpu hours over the same time interval. While a full simulation may include thousands of subhaloes, we have demonstrated that it is possible to vary the parameters and rerun multiple versions of a single subhalo in a small fraction of the time.

5 CONCLUSIONS

We have demonstrated the power of using the SCF expansion method to approximate a dark matter halo. While much work has previously been carried out using the SCF technique in expansion codes to calculate the force in an N-body simulation, this is the first time it has been applied to describe an already simulated dark matter halo. Using a small number of basis functions, the SCF technique offers a way

¹ On a 2.2 GHz AMD Opteron (AMD Opteron 175)

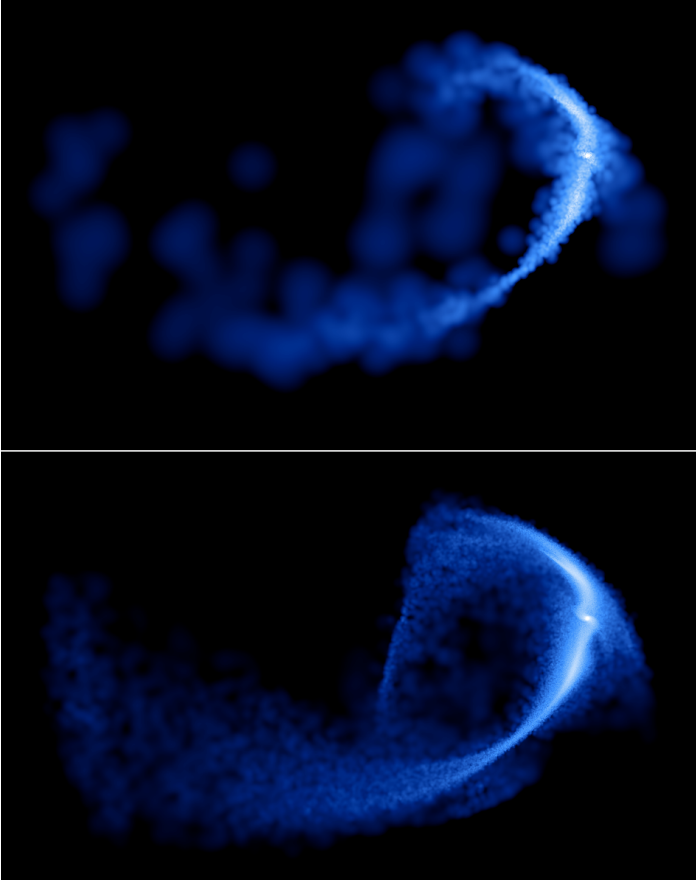


Figure 13. The smoothed density of the resimulated subhalo after 5 Gyrs at $z = 0$ using the SCF expansion. *Upper picture:* the low resolution realisation subhalo containing 6000 particles. *Lower picture:* the high resolution realisation subhalo containing 10^6 particles.

to approximate the time-evolving potential. A set of coefficients can be calculated once from the simulation and then serve as a realistic approximation of a halo. It is simple to integrate orbits within the SCF potential approximation and, as a first test, we focused on particle and subhalo orbits.

Using the SCF method to represent a dark matter halo, however, has some limitations. The potential is fixed and unable to react to objects within it. New elements placed in the simulation, such as additional subhaloes, cannot modify the halo potential. This could be especially problematic when considering galaxies and the adiabatic contraction that the presence of baryons is expected to produce. The second major limitation is the lack of dynamical friction that should be present in the equation of motions. Subhaloes orbiting within the expansion are missing the effect of this force that would make their orbits decay. While it is possible to add in dynamical friction analytically, this requires assuming a model of subhalo evolution to estimate the mass and size of the subhalo.

Through application of the SCF method to an Aquarius simulated dark matter halo we have demonstrated that:

- An SCF expansion of a dark matter halo can approximate the halo well enough to recover the radial component

of the force to within 1% using only a few radial basis functions.

- It is possible to integrate orbits within the expansions and reproduce overall population trends. For individual orbits the degree of success is varied. For orbits that are near circular and stay within the central 20 kpc of the halo we can accurately follow their path over several dynamical timescales.

- Subhaloes orbit like point masses. Their extended nature and tidal streams have little or no effect on their orbits. The orbits of subhaloes are not simple planar orbits but involve complicated changes in orientation and scattering from the halo centre and other subhaloes.

- The method can reproduce the structural evolution of individual subhaloes. To obtain similar evolution for a particular subhalo we need to match its orbit, which requires a full potential expansion. To match the correct overall population evolution we do not need the full SCF expansion, but only the radial terms are required to obtain the correct radial mass distribution. Not including the angular terms greatly speeds up the force evaluation.

We have been able to introduce new objects, such as subhaloes into the SCF potential; we find an evolution consistent with that which would have taken place if the subhaloes had been present in the original Aquarius simulation. The technique allows us to simulate subhaloes with much higher resolution than in the original simulation and resolve features in the tidally stripped streams in great detail.

While the SCF technique has some limitations it offers a powerful way of improving current models of galaxy formation. The standard simple spherically symmetric profiles often used to represent the dark matter halo when modelling dynamical processes involving orbits miss important effects related to the triaxiality of haloes and the evolution of the potential. In order to build more realistic models it is necessary, as we have shown, to use more sophisticated representations of dark matter haloes such as the ones the SCF technique offers. There is a large number of possible applications for this technique and we have briefly explored only a few of these in this paper.

ACKNOWLEDGMENTS

The simulations for the Aquarius Project were carried out at the Leibniz Computing Centre, Garching, Germany, at the Computing Centre of the Max-Planck-Society in Garching, at the Institute for Computational Cosmology in Durham, and on the STELLA supercomputer of the LOFAR experiment at the University of Groningen. BJL would like to thank Andrew Cooper for useful discussions and suggestions. He is supported by an STFC postgraduate studentship. CSF acknowledges a Royal Society Wolfson Research Merit award. This work was supported in part by an STFC rolling grant to the ICC.

REFERENCES

- Abadi M. G., Navarro J. F., Fardal M., Babul A., Steinmetz M., 2010, MNRAS, 407, 435

- Abramowitz M., Stegun I. A., 1964, Handbook of Mathematical Functions with Formulas, Graphs, and Mathematical Tables, ninth dover printing, tenth gpo printing edn., Dover, New York
- Adams F. C., Bloch A. M., 2005, *ApJ*, 629, 204
- Allgood B., Flores R. A., Primack J. R., Kravtsov A. V., Wechsler R. H., Faltenbacher A., Bullock J. S., 2006, *MNRAS*, 367, 1781
- Angulo R. E., Lacey C. G., Baugh C. M., Frenk C. S., 2009, *MNRAS*, 399, 983
- Benson A. J., Lacey C. G., Frenk C. S., Baugh C. M., Cole S., 2004, *MNRAS*, 351, 1215
- Bett P., Eke V., Frenk C. S., Jenkins A., Helly J., Navarro J., 2007, *MNRAS*, 376, 215
- Bett P., Eke V., Frenk C. S., Jenkins A., Okamoto T., 2010, *MNRAS*, 404, 1137
- Boylan-Kolchin M., Ma C., Quataert E., 2008, *MNRAS*, 383, 93
- Bullock J. S., Johnston K. V., 2005, *ApJ*, 635, 931
- Chandrasekhar S., 1943, *ApJ*, 97, 255
- Choi J., Weinberg M. D., Katz N., 2009, *MNRAS*, 400, 1247
- Clutton-Brock M., 1973, *Ap&SS*, 23, 55
- Debattista V. P., Moore B., Quinn T., Kazantzidis S., Maas R., Mayer L., Read J., Stadel J., 2008, *ApJ*, 681, 1076
- Diemand J., Kuhlen M., Madau P., Zemp M., Moore B., Potter D., Stadel J., 2008, *Nature*, 454, 735
- Earn D. J. D., Sellwood J. A., 1995, *ApJ*, 451, 533
- Frenk C. S., White S. D. M., Efstathiou G., Davis M., 1985, *Nature*, 317, 595
- Hayashi E., Navarro J. F., Springel V., 2007, *MNRAS*, 377, 50
- Hernquist L., 1990, *ApJ*, 356, 359
- Hernquist L., Ostriker J. P., 1992, *ApJ*, 386, 375
- Kazantzidis S., Magorrian J., Moore B., 2004, *ApJ*, 601, 37
- Law D. R., Majewski S. R., Johnston K. V., 2009, *ApJ*, 703, L67
- Navarro J. F., Frenk C. S., White S. D. M., 1996, *ApJ*, 462, 563
- , 1997, *ApJ*, 490, 493
- Navarro J. F., Ludlow A., Springel V., Wang J., Vogelsberger M., White S. D. M., Jenkins A., Frenk C. S., Helmi A., 2010, *MNRAS*, 402, 21
- Peñarrubia J., Benson A. J., 2005, *MNRAS*, 364, 977
- Peñarrubia J., Benson A. J., Martínez-Delgado D., Rix H. W., 2006, *ApJ*, 645, 240
- Springel V., 2005, *MNRAS*, 364, 1105
- Springel V., Wang J., Vogelsberger M., Ludlow A., Jenkins A., Helmi A., Navarro J. F., Frenk C. S., White S. D. M., 2008a, *MNRAS*, 391, 1685
- Springel V., White S. D. M., Frenk C. S., Navarro J. F., Jenkins A., Vogelsberger M., Wang J., Ludlow A., Helmi A., 2008b, *Nature*, 456, 73
- Springel V., White S. D. M., Tormen G., Kauffmann G., 2001a, *MNRAS*, 328, 726
- Springel V., Yoshida N., White S. D. M., 2001b, *New A*, 6, 79
- Stadel J., Potter D., Moore B., Diemand J., Madau P., Zemp M., Kuhlen M., Quilis V., 2009, *MNRAS*, 398, L21
- Taylor J. E., Babul A., 2001, *ApJ*, 559, 716
- Vogelsberger M., White S. D. M., 2010, *ArXiv e-prints*
- Weinberg M. D., 1996, *ApJ*, 470, 715
- , 1999, *AJ*, 117, 629
- White S. D. M., Rees M. J., 1978, *MNRAS*, 183, 341
- Zentner A. R., Bullock J. S., 2003, *ApJ*, 598, 49